Reconstructing the Substrate for Uracil DNA Glycosylase: Tracking the Transmission of Binding Energy in Catalysis†

Yu Lin Jiang and James T. Stivers*

Department of Pharmacology and Molecular Sciences, Johns Hopkins University School of Medicine, 725 North Wolfe Street, Baltimore, Maryland 21205-2185

Received March 27, 2001

ABSTRACT: The DNA repair enzyme uracil DNA glycosylase (UDG) is a powerful *N*-glycohydrolase that cleaves the glycosidic bond of deoxyuridine in DNA. We have investigated the role of substrate binding energy in catalysis by systematically dismantling the optimal substrate $Ap^{+1}\mathbf{U}pA^{-1}pA^{-2}$ by replacing the nucleotides at the +1, −1, or −2 position with a tetrahydrofuran abasic site nucleotide (D), a 3-hydroxypropyl phosphodiester spacer (S), a phosphate monoester (p), or a hydroxyl group (h). Contrary to previous reports, the minimal substrate for UDG is 2′-deoxyuridine (h**U**h). UDG has a significant catalytic efficiency (CE) for h**U**h of 4×10^7 M^{-1} [$CE = (k_{cat}/K_m)(1/k_{non})$, where k_{non} is the rate of the spontaneous hydrolysis reaction of h**U**h at 25 °C]. Addition of +1 and −1 phosphate monoanions to form p**U**p increases k_{cat}/K_m by 45-fold compared to that of h**U**h. The k_{cat}/K_m for p**U**p, but not p**U** or **U**p, is found to decrease by 20-fold over the pH range of 6−9 with a pK_a of 7.1, which is identical to the pK_a values for deprotonation of the +1 and −1 phosphate groups determined by the pH dependence of the ^{31}P NMR chemical shifts. This pH dependence indicates that binding of the p**U**p tetraanion is disfavored, possibly due to unfavorable desolvation or electrostatic properties of the highly charged +1 and −1 phosphate groups. Addition of flexible hydroxypropyl groups to the +1 and −1 positions to make Sp**U**pS increases k_{cat}/K_m by more than 10^5-fold compared to that of h**U**h, which is a 20-fold greater effect than observed with rigid D substituents in these positions (i.e., Dp**U**pD). The −2 phosphoester or nucleotide is found to increase the reactivity of trimer substrates with rigid furanose rings or nucleotides in the +1 and −1 positions by 1300−270000-fold (i.e., Dp**U**pD → Dp**U**pDpA or Ap**U**pA → Ap**U**pApA). In contrast, the −2 nucleotide provides only an 8-fold rate enhancement when appended to the substrate containing the more flexible +1 and −1 S substituents (Sp**U**pS → Sp**U**pSpA). These context-dependent effects of a −2 nucleotide are interpreted in terms of a mechanism in which the binding energy of this "handle" is used drive the rigid +1 and −1 A or D substituents into their binding pockets, resulting in a net catalytic benefit of −4.3 to −7.5 kcal/mol. Taken together, these results systematically track how UDG uses distant site binding interactions to produce an overall *four billion-fold* increase in CE compared to that of the minimal substrate h**U**h.

Despite nearly one hundred years of intense interest in the nature of the forces that give rise to enzyme rate accelerations and specificity, the basic question of how an enzyme acts so effectively on its specific substrate and so ineffectively on a similar poor substrate is still hotly debated (*1*−*3*). This debate exists despite the tremendous surge of high-resolution structures of enzymes and their complexes with substrate analogues, products, and even transition-state mimics (*4*−*6*). One might assume that such atomic level insights into the interactions between the enzyme and the substrate in its ground-state and transition-state forms would provide most of the information necessary to understand specificity and catalysis. However, the continuing difficulties in using structural information to directly design specific and tight binding inhibitors of enzymes highlights the general problem that *observed* interactions cannot be easily translated into binding energies, the basic currency of enzymatic specificity and catalysis (*3*). Such difficulties in linking structure and function are exacerbated in enzymes that utilize induced fit mechanisms, because it is likely that the observed interactions may be used to drive a conformational change, or cause destabilization of the ES complex, to lower the activation barrier of the chemical transformation. Therefore, in such cases, assessment of the energetic contribution of the observed interactions must rely on other approaches that are capable of dissecting the linkage between structure and function.

A provocative and extreme example of induced fit specificity and ground-state destabilization is found in the recently determined crystal structure of the DNA repair enzyme uracil DNA glycosylase (UDG) in complex with DNA containing the nonreactive C-glycoside deoxyuridine analogue, pseudodeoxyuridine (ΨdU, Figure 1) (*5*). UDG is a powerful *N*-glycohydrolase that cleaves the glycosidic bond of deoxyuridine in DNA, resulting in the products uracil and abasic DNA. The structural finding depicted schemati-

† This work was supported by NIH Grant RO1 GM56834 (J.T.S.).

* To whom correspondence should be addressed. Phone: (410) 502-2758. Fax: (410) 955-3023. E-mail: jstivers@jhmi.edu.

10.1021/bi010622c CCC: $20.00
Published on Web 05/31/2001

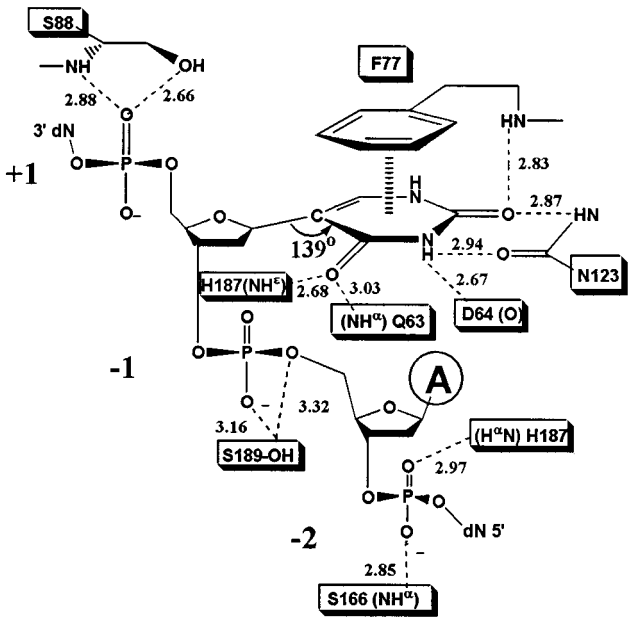

FIGURE 1: Key substrate interactions of UDG in the Michaelis complex as determined from the crystal structure of human UDG in complex with DNA containing the nonreactive C-glycoside uracil analogue ψdU (*5*). Phosphodiester interactions with three conserved serine residues (Ser88, Ser189, and Ser166) and the backbone amide of His187 are shown. These interactions are postulated to rigidly hold the furanose sugar while Phe77 forcibly stacks onto the uracil ring, thereby bending the C1′−N1−C4 angle by 41° from its normal 180° arrangement. Other interactions that hold the uracil (or ψU) base in position are hydrogen bonds from His187 NH$^{\epsilon}$ and Gln63 NHα to uracil O2, and side chain amide hydrogen bonds from Asn123 to uracil O4 and H3.

cally in Figure 1 suggests that the normally trigonal planar C1 of ΨdU is distorted to a tetrahedral geometry upon binding to UDG, providing perhaps the most extreme example of ground-state strain yet observed in any crystallographic study of an enzyme. The distortion is apparently brought about by serine clamps that pinch the 3′ and 5′ phosphodiesters flanking the deoxyuridine, which forces the uracil base into a stacking interaction with a phenylalanine side chain. As proposed by Parikh et al., the mechanistic role for this destabilization is to provide an enhanced electronic pathway for the lone pair electrons on O4′ to uracil O2, thereby facilitating a dissociative transition state for glycosidic bond cleavage. The short half-life for cleavage of the glycosidic bond of deoxyuridine in DNA by UDG (5 ms) requires that the enzyme lower the activation barrier by 16 kcal/mol with respect to that of the uncatalyzed reaction ($t_{1/2}$ = 220 years) (*7*, *8*). According to this proposal, glycosidic bond strain and its relief in the transition state provide the majority of the 16 kcal/mol catalytic power of UDG.

Additional insights into the UDG reaction mechanism have been obtained from solution NMR, Raman spectroscopy, mutagenesis, and kinetic isotope effect studies. Heteronuclear NMR studies have established that the N1 pK_a of the uracil leaving group is lowered by 3.4 log units through formation of a short, strong hydrogen bond between a neutral active site histidine and uracil O2 in the product complex (*9*, *10*). In addition, off-resonance Raman spectroscopy studies of several UDG−DNA complexes have confirmed the presence of a stable uracil anion in the product complex, confirming a catalytic role for enzymatic stabilization of the uracil leaving group by ~5 kcal/mol in the transition state (*11*). In addition, the Raman studies have revealed a strong polarization of the deoxyuridine O2 and O4 carbonyl groups in the ES complex through hydrogen bonding to backbone and side chain amide groups (Figure 1), suggesting a type of ground-state activation different from the crystallographic proposal. Provocatively, these Raman studies, which utilized 2′-β-fluoro-2′-deoxyuridine substrate analogues, provided no evidence of an unusual electronic rearrangement of the uracil ring in the ES complex, such as that suggested in the UDG complex with deoxypseudouridine DNA. Moreover, deletion of the conserved serine residues that were proposed to strain the glycosidic bond (Figure 1) resulted in only modest effects on the activation barrier (<500-fold), providing no support for a large strain contribution to catalysis involving these groups (*7*). Finally, recent kinetic isotope effect studies have established that the reaction proceeds through a discrete oxocarbenium ion intermediate, which is likely stabilized by an enforced planar conformation of the deoxyribose ring, and a sandwich of negative charges provided by the nascent uracil O2 anion and a conserved active site aspartic acid (*12*).

Given the importance of the reaction catalyzed by UDG, and the surprising structure of the ES complex as suggested by the crystallographic model, we were compelled to investigate the role of noncovalent substrate binding interactions in catalysis. In this study, we reconstruct the optimal substrate for UDG in search of the energetic contributions from these binding interactions. Although such an approach can only yield the net catalytic effect of a substituent group,[1] the results provide a consistent picture of how distant site binding interactions facilitate catalysis by up to −13 kcal/mol over the minimal substrate deoxyuridine.

EXPERIMENTAL PROCEDURES

Materials. The DNA substrates were synthesized using standard phosphoramidite chemistry with an Applied Biosystems 390 synthesizer. The nucleoside phosphoramidites, 5′ chemical phosphorylating reagent, universal support CPG, and 3′-phosphate CPG were purchased from Glen Research (Sterling, VA). Deoxyuridne and 5′-dUMP were from Sigma Chemicals. The substrates Sp**U**pS and Dp**U**pD were synthesized using the universal support CPG and the appropriate 3′-phosphoramidite. The substrates p**U**, **U**p, and p**U**p were synthesized using the 3′-phosphate CPG and/or the 5′-chemical phosphorylating reagent, and were released from the support using concentrated NH_4OH at 80 °C for 8 h. After synthesis and deprotection, the phosphodiester oligonucleotides were purified by anion exchange HPLC and desalted by C-18 reversed phase HPLC (Phenomenex Aqua column). The purity and nucleotide composition of the DNA were assessed by analytical reversed phase HPLC and MALDI[2] or electrospray mass spectrometry. The concentra-

[1] The observed energetic consequences due to the removal or addition of a substituent group must *not* be interpreted as the intrinsic binding interaction of the individual group. The effects that are measured here are context specific, and reflect the net energetic contribution of the substituent in the given substrate context (for an excellent discussion of such effects, see ref *3*).

[2] Abbreviations: *e*UDG, *Escherichia coli* uracil DNA glycosylase; *h*UDG, human uracil DNA glycosylase; 2′-FU, 2′-fluoro-2′-deoxyuridine nucleotide; **P**, 2-aminopurine; MALDI, matrix-assisted laser desorption ionization mass spectrometry; TMN, standard buffer consist-

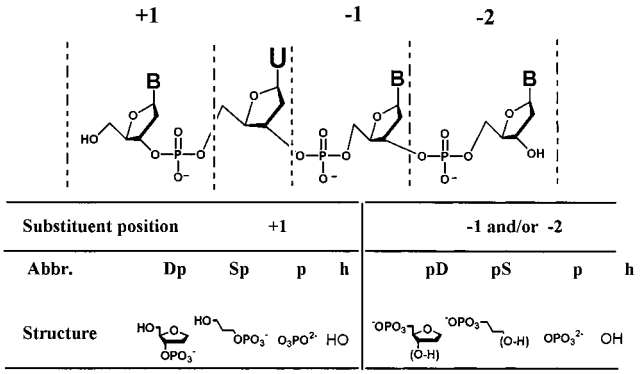

FIGURE 2: Reconstruction substrates and nomenclature. In the text, the Dp and pD substituents and the Sp and pS substituents are sometimes termed "D" and "S" for simplicity.

tions were determined by UV absorption measurements at 260 nm, using the pairwise extinction coefficients for the constituent nucleotides (*13*). The purification of *e*UDG has been described previously (*14*, *15*).

Steady-State Kinetic Measurements and Cleavage Assays. The steady-state kinetics of uracil glycosidic bond cleavage were determined at 25 °C in TMN buffer [10 mM Tris-HCl (pH 8.0), 2.5 mM $MgCl_2$, 25 mM NaCl, and 10 μg/mL BSA] using a new HPLC-based assay with UV detection at 260 nm (Waters 486 UV−vis detector). Twenty microliter samples of the reaction mixtures (100 μL) were injected directly onto the HPLC column using a flow rate of 1 mL/min. A Phenomenex Aqua reversed phase C-18 HPLC column (250 mm × 4.60 mm, 5 μm) with the following solvent systems was used: 4mer substrates, isocratic elution with 11% CH_3CN in 0.1 M aqueous TEAA; mononucleotide, dinucleotide, and trinucleotide substrates containing D or S, isocratic elution with 1.5% CH_3CN in 0.03 M aqueous TEAA; and other 3mer substrates, isocratic elution with 9.8% CH_3CN in 0.1 M aqueous TEAA.

The steady-state kinetic parameters k_{cat} and k_{cat}/K_m were obtained from plots of the observed rate constants (k_{obsd}) versus substrate concentration ($[S]_{tot}$) using a standard hyperbolic kinetic expression and the program *Grafit 4* (*16*) according to eqs 1 and 2:

$$k_{obsd} = (1/\Delta t) \times 1/[UDG]_{tot} \times [S]_0[I^P/(I^P + I^S R)] \quad (1)$$

$$k_{obsd} = k_{cat}/(K_m + [S]) \quad (2)$$

In eq 1, $[S]_0$ is the initial substrate concentration, $[UDG]_{tot}$ is the total UDG concentration, I^S and I^P are the integrated peak areas for the substrate and abasic product at time Δt, respectively, and $R = \epsilon^P/\epsilon^S$, the ratio of the molar extinction coefficients for the abasic product and substrate. In all cases, seven to ten rate measurements at different substrate concentrations were performed to define the fits to eq 2. Typically, each determination of k_{obsd} consisted of three independent determinations of P concentration at times Δt, which were averaged.

For some weak binding substrates that contained only a uracil chromophore (see Figure 2), the rate showed only a linear dependence on the substrate concentration, and thus, only k_{cat}/K_m values could be obtained. In these cases, the uracil peak was integrated and compared directly with the integrated area of a uracil standard. The k_{cat}/K_m values were obtained from the slopes of linear plots of the observed rates versus substrate concentration (four to five concentrations) after dividing by the UDG concentration. In some cases, the time course of uracil product formation was followed for as long as 24 h. For these slow reactions (h**U**h, h**U**p, p**U**h, p**U**p, h**U**pD, and Dp**U**h), all the components were filter sterilized to prevent bacterial growth, and glycerol was completely removed from the enzyme stock solution to prevent interference in the HPLC assay. In addition, the h**U**h substrate stock was HPLC purified before the reaction with UDG to remove trace amounts of uracil (<0.1%). The substrate concentrations were in the range of 100−600 μM, and the UDG concentration was in the range of 10−20 μM. Control experiments were performed to show that in the absence of UDG no detectable uracil was formed over the same time period.

pH Dependence of k_{cat}/K_m. For wild-type UDG, the pH dependencies of the rate of glycosidic bond cleavage for substrates p**U**p, p**U**, Up, and Sp**U**pS were determined using the HPLC kinetic assay in the pH range of 6−10 at 25 °C with the following buffers (all 10 mM containing 20 mM NaCl): NaMES at pH 6.0−6.5, NaHEPES at pH 6.5−7.5, Tris-HCl at pH 7.5−8.5, NaCHES at pH 8.5−9.5, and NaCAPS at pH 9.5−10. The pH dependence of the observed k_{cat}/K_m was fitted to eq 3 by nonlinear regression analysis using *Grafit 4* (*16*)

$$k_{cat}/K_m^{obsd} = [k_{cat}/K_m^{min} + k_{cat}/K_m^{max}(10^{pH-pK_a})]/(10^{pH-pK_a} + 1) \quad (3)$$

where k_{cat}/K_m^{min} and k_{cat}/K_m^{max} are the limiting rate constants at high and low pH, respectively.

pH Titrations Using ^{31}P NMR. One-dimensional ^{31}P NMR experiments were performed at 25 °C with a Bruker Avance 500 MHz NMR spectrometer using a triple-resonance HCP probe. The sample included 1 mM p**U**p and 20 mM NaCl in 0.75 mL of D_2O. The spectra were recorded with the following acquisition parameters: a spectral width of 2022 Hz, the carrier frequency set at 0 ppm relative to external 85% H_3PO_4, an acquisition time of 1 s, and a relaxation delay of 1 s. The FIDs consisting of 2K complex points were processed using 20 Hz line broadening. Titrations were performed by adding small aliquots of 0.1 M NaOD or DCl. The pK_a values for the 3′- and 5′-phosphates of p**U**p were determined by following the ^{31}P chemical shift changes as a function of pH* in D_2O. The apparent electrode readings were not corrected for deuterium isotope effects, because the glass electrode effect is expected to approximately cancel the increased pK_a of the phosphate groups in D_2O (*17*). This may introduce an uncertainty of ±0.1 unit in the true group pK_a value in water (*23*), but this uncertainty has no impact on the conclusions in this work. The titration data were fitted by nonlinear regression analysis to eq 4

$$\delta(ppm) = [\delta_1 + \delta_2(10^{pH-pK_a})]/(10^{pH-pK_a} + 1) \quad (4)$$

where δ_1 and δ_2 are the limiting chemical shifts at low and high pH, respectively. The phosphorus chemical shift assignments were made using a two-dimensional $^1H-^{31}P$ CPMG-HSQC experiment,[3] to correlate the 3′- and 5′-protons to the corresponding phosphorus atoms.

ing of 10 mM Tris-HCl (pH 8.0), 20 mM NaCl, and 2.5 mM $MgCl_2$.

Metal Ion Dependence of k_{cat}/K_m. The binding of Mg^{2+} and Na^+ ions to the phosphate groups of p**U**p, p**U**, **U**p, and S**U**S was investigated by measuring the extent of inhibition of the observed k_{cat}/K_m as a function of salt concentration. For titrations with $MgCl_2$, the data were fitted to eq 5, which assumes a single inhibitory Mg^{2+} binding site with a dissociation constant K_D^{Mg}

$$k/k_o = (1 + k_+/k_o[Mg^{2+}]/K_D^{Mg})/(1 + [Mg^{2+}]/K_D^{Mg}) \quad (5)$$

where k is the observed k_{cat}/K_m at a given $MgCl_2$ concentration and k_o and k_+ are the limiting k_{cat}/K_m values at zero and infinite $MgCl_2$ concentrations, respectively. Under the conditions that were employed, where binding of substrate is in rapid equilibrium and $[S] \ll K_m$, the measured K_D^{Mg} should be equal to a true dissociation constant of the metal ion from the free substrate.

For the titrations with NaCl, which showed no evidence for saturation, the data were fitted to eq 6

$$\log k_{cat}/K_m^{obsd} = S \log[NaCl] + A \quad (6)$$

where A is the extrapolated value of $\log k_{cat}/K_m^{obsd}$ at a 1 M standard state of sodium chloride and S is the slope or power dependence of $\log k_{cat}/K_m^{obsd}$ on salt concentration (*18*).

RESULTS AND DISCUSSION

General Approach. The goal of this work is to quantify the substrate binding interactions that contribute to the tremendous catalytic power of UDG. We have taken a "substrate reconstruction" approach to this problem in which functional groups comprising the optimal 4mer substrate, $Ap^{+1}\mathbf{U}pA^{-1}pA^{-2}$ (Figure 2), were removed until a minimal substrate (h**U**h) was obtained (see Figure 2 for structures and nomenclature). We then systematically add back a phosphate monoester (p), a 3-hydroxypropyl phosphodiester spacer (pS or Sp), or a tetrahydrofuran abasic site nucleotide (pD or Dp), at the +1, −1, or −2 position to evaluate the net contributions of these functionalities to catalysis. We report the catalytic efficiencies (CE) of the various constructs as the ratio $(k_{cat}/K_m)/k_{non}$, where a k_{non} of 10^{-10} s^{-1} is the extrapolated spontaneous rate of hydrolysis of dU at 25 °C and pH 7.5 (*19*, *20*).[4] As previously noted (*7*), comparisons using k_{cat}/K_m are most appropriate because this constant describes the activation barrier for proceeding from the free substrate to the transition state of the chemical step. Comparisons using k_{cat} are less useful because of possible contributions from nonproductive binding, and because product release becomes rate-limiting for the very best substrates of UDG (*7*, *14*, *21*).

Kinetic Studies. Representative HPLC traces for uracil (**U**) cleavage from the substrate Ap**U**pApA and h**U**h by UDG are shown in panels A and B of Figure 3, respectively.

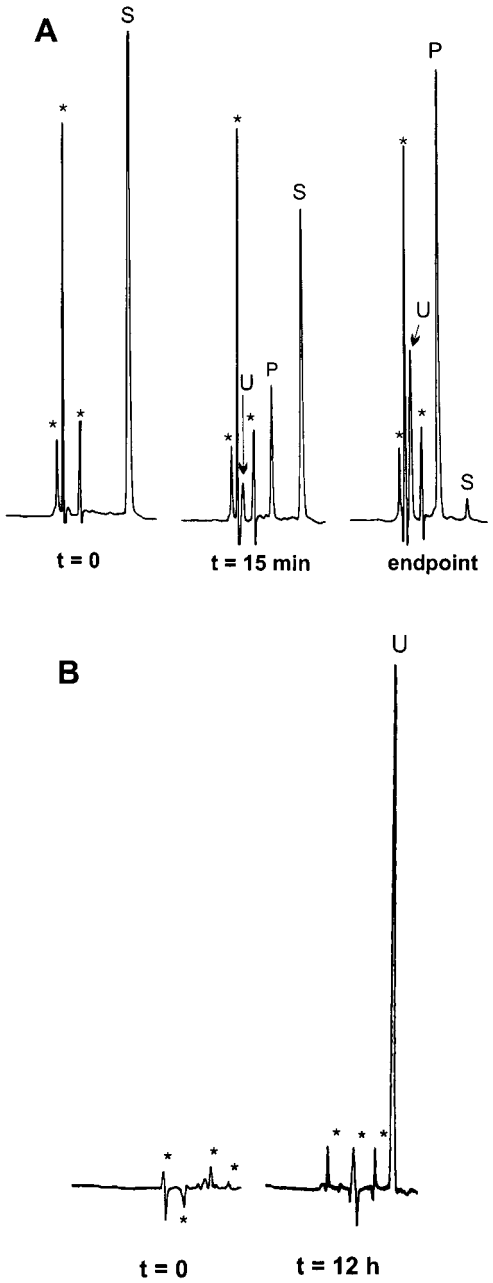

FIGURE 3: (A) HPLC traces showing the time course for the UDG-catalyzed cleavage of uracil (U) from the 2-aminopurine-containing substrate Ap**U**pPpA (S). Integration of the abasic product peak (P) was used to determine the intial rate. Conditions: [Ap**U**pPpA] = 1 μM, [UDG] = 0.25 nM. Twenty microliters of a 100 μL reaction mixture was injected, and the absorbance at 260 nm was monitored. The peaks marked with asterisks are buffer peaks present in all the samples. (B) Representative HPLC trace showing the amount of uracil released from 600 μM h**U**h after incubation for 12 h with UDG (20 μM) in TMN buffer. A control injection at time zero is also shown.

Although both the uracil and abasic products are well separated from the Ap**U**pApA substrate using this reversed phase system, the extinction coefficient for the abasic product is greater, and therefore provides the most useful signal for peak integration and determination of the initial rates. However, for h**U**h and several derivatives with p, D, and S substituents (Figure 2 and Table 1), the absence of a UV signal for the abasic product required monitoring of the uracil peak by HPLC (Figure 3B). In some cases, the measured initial rates displayed a hyperbolic substrate concentration

[3] B. Luy and J. P. Marino, unpublished observations.

[4] The spontaneous hydrolysis rate for deoxyuridine at pH 7.0 has been previously studied over the temperature range of 95−75 °C, from which an activation energy of 32.1 kcal/mol was determined (*19*, *20*). This allowed calculation of the spontaneous rate of 10^{-10} s^{-1} at 25 °C by extrapolation using the Arrhenius equation. The rate of dU hydrolysis was independent of pH and the nature and concentration of the buffer in the pH range of 3−8, indicating that the nucleophile is water, as in the enzymic reaction (*19*, *20*).

Table 1: Kinetic Parameters for Ap**U**pApA and Truncated Substrates[a]

substituted position	substrate	k_{cat} (s^{-1})	K_m (μM)	k_{cat}/K_m (M^{-1} s^{-1})[b]	CE[c] (M^{-1})
+1	Ap**U**pApA	15.8 ± 0.3	1.0 ± 0.1	(15.2 ± 1.4) × 10^6	1.5 × 10^{17}
	Dp**U**pApA	14.6 ± 0.6	3.2 ± 0.4	(4.6 ± 0.6) × 10^6	4.6 × 10^{16}
	Sp**U**pApA	1.3 ± 0.1	0.9 ± 0.3	(1.4 ± 0.4) × 10^6	1.4 × 10^{16}
	p**U**pApA	0.13 ± 0.00	1.9 ± 0.1	(0.07 ± 0.001) × 10^6	7 × 10^{14}
	h**U**pApA	0.25 ± 0.02	53.5 ± 7.8	(0.005 ± 0.001) × 10^6	5 × 10^{13}
−1	Ap**U**pDpA	9.4 ± 0.4	179 ± 72	(0.05 ± 0.01) × 10^6	5 × 10^{14}
	Ap**U**pSpA	2.6 ± 0.1	61.0 ± 5.5	(0.04 ± 0.005) × 10^6	4 × 10^{14}
+1, −1	Dp**U**pDpA	41.5 ± 5.6	974 ± 158	(0.05 ± 0.001) × 10^6	5 × 10^{14}
	Sp**U**pSpA	0.10 ± 0.01	18.6 ± 4.7	(0.005 ± 0.001) × 10^6	5 × 10^{13}
−2	Ap**U**pApD	32.1 ± 2.3	67.1 ± 9.6	(0.57 ± 0.01) × 10^6	5.7 × 10^{15}
	Ap**U**pApS	25.2 ± 2.7	41.3 ± 8.4	(0.58 ± 0.02) × 10^6	5.8 × 10^{15}
	Ap**U**pAp	22.9 ± 0.5	20.0 ± 1.2	(1.14 ± 0.07) × 10^6	1.1 × 10^{16}
	Ap**U**pAh[c]			56 ± 5	5.6 × 10^{11}
+1, −1	Dp**U**pD[c]			35 ± 4	3.5 × 10^{11}
	Sp**U**pS			700 ± 75	7 × 10^{12}
	Sp**U**p			9.0 ± 1	9 × 10^{10}
	p**U**pS			10 ± 1	1 × 10^{11}
	Dp**U**h			0.62 ± 0.07	6 × 10^9
	h**U**pD			0.078 ± 0.009	7.8 × 10^8
	Sp**U**h			0.42 ± 0.04	4.2 × 10^9
	h**U**pS			1.0 ± 0.07	1 × 10^{10}
+1,−1	p**U**p^{-2}[d]			0.19 ± 0.01	1.9 × 10^9
	p**U**p^{-4}[d]			0.0065 ± 0.0006	6.5 × 10^7
	p**U**p[e]			0.0096 ± 0.0009	9.6 × 10^7
	p**U**h			0.062 ± 0.007	6.2 × 10^8
	h**U**p			0.0073 ± 0.0006	7.3 × 10^7
	h**U**h			0.0042 ± 0.0003	4.2 × 10^7

[a] Kinetic parameters were determined at 25 °C in TMN buffer at pH 8.0. [b] Only k_{cat}/K_m was determined for some reactions due to the high K_m values. [c] Catalytic efficiency, CE = $(k_{cat}/K_m)/k_{non}$, where k_{non} (=10^{-10} s^{-1}) is the spontaneous rate of hydrolysis of deoxyuridine (h**U**h) (*19*, *20*). [d] These kinetic constants for p**U**p^{-2} and p**U**p^{-4} (measured in 10 mM buffer with 20 mM NaCl) were extrapolated from the low- and high-pH asymptotes of the pH dependence of k_{cat}/K_m according to eq 3 (see also Figure 5A). [e] This value for p**U**p was obtained using the standard TMN buffer conditions at pH 8.0 (see the text).

dependence, from which the steady-state kinetic parameters k_{cat}, k_{cat}/K_m, and K_m were well-determined (Figure 4A). However, due to the weak binding of some of the substrates, only k_{cat}/K_m values were measured from the slopes of the linear concentration dependence of the observed rates on substrate concentration (Figure 4B). The relative steady-state kinetic parameters and catalytic efficiencies (CE) for the various substrates are reported in Table 1.

Minimal Substrate for UDG. Although it has been previously reported and widely assumed that UDG cannot remove uracil from a 3′-terminal position of DNA (*22*), we have found here that the minimal substrate for UDG is deoxyuridine (h**U**h, Figure 4B and Table 1). The CE value for h**U**h is more than a billion-fold lower than that of the best substrate, Ap**U**pApA; however, the k_{cat}/K_m for h**U**h is still (4 × 10^7)-fold greater than k_{non}. Thus, in the complete absence of phosphodiester handles, or +1, −1, and −2 nucleotides, UDG can achieve a significant catalytic efficiency. Measurement of the CE for h**U**h allows us to quantify the relative effects of adding p, S, D, and nucleotide substituents to this minimal scaffold as described below.

Catalytic Contribution of the +1 and −1 Phosphoesters in the Context of a 3mer Scaffold. To test the binding energy contributions of the +1 and −1 phosphoester substituents in the transition state, both individually and combined, we constructed the substrates p**U**h, h**U**p, p**U**p, Sp**U**h, h**U**pS, Sp**U**pS, h**U**pD, Dp**U**h, and Dp**U**pD (Figure 2 and Table 1). This series of substituents allows evaluation of the roles of phosphate charge (i.e., monoanion or dianion), flexibility of the phosphodiester substituent (S or D), and the interaction energies for simultaneous binding of the +1 and −1 groups (vida infra). Addition of a single +1 and −1 phosphate dianion (p) produces modest 15- and 1.7-fold increases in CE compared to that of h**U**h, respectively. Using the standard TMN buffer conditions at pH 8.0, the simultaneous addition of a +1 and −1 phosphate to form p**U**p^{-4} increases the CE by only 2-fold compared to that of h**U**h, which is a 7-fold smaller increase compared to that of p**U**. This finding indicates that the addition of a −1 phosphate totally disrupts the favorable interaction energy with the +1 phosphate, and implies absolute negative cooperativity in binding these two phosphate groups by the enzyme. Further investigation of the pH and metal ion dependence described below establishes that this *apparent* negative cooperativity is due to selective inhibition by Mg^{2+} of the reaction of p**U**p^{-4}, and the −4 charge state of p**U**p at pH 8.0, which introduces an unfavorable electrostatic effect as compared to **U**p^{-2} and p**U**$^{-2}$ (vida infra).

Addition of a single +1 and −1 phosphodiester linkage to form h**U**pD, Dp**U**h, h**U**pS, and Sp**U** results in 20−200-fold increases in CE, while the double-phosphodiester substrates, Dp**U**pD and Sp**U**pS, show enormous 8000- and 170000-fold increases in CE compared to that of h**U**h (Table 1). The increases in CE upon introduction of two phosphodiester groups are greater than expected from simple multiplicative effects arising from binding the individual +1 and −1 phosphodiesters, and indicate energetic cooperativity (vida infra). The 20-fold larger CE for Sp**U**pS compared to Dp**U**pD corresponds to a −1.8 kcal/mol catalytic advantage for a smaller and more flexible phosphodiester linkage at the +1 and −1 positions in these trimer substrates.

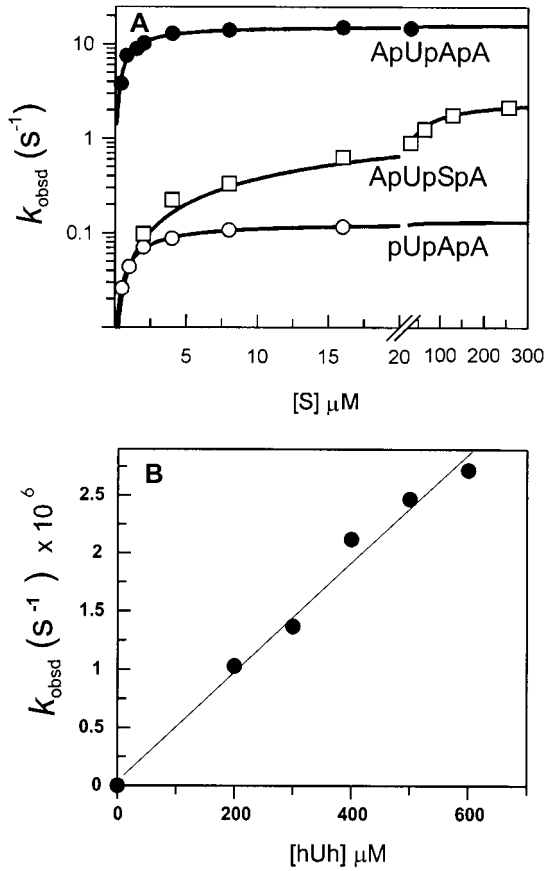

FIGURE 4: (A) Hyperbolic substrate concentration dependence of the observed steady-state rates of uracil cleavage from the indicated substrates. The lines are the fits to eq 2. (B) Linear concentration dependence of the reaction of h**U**h with UDG. The solid line is the linear regression fit to the data. The slope gives a k_{cat}/K_m of 4.2×10^{-3} M^{-1} s^{-1}. The full kinetic results are reported in Table 1.

Why are +1 and −1 Phosphodiesters More Reactive Than Phosphate Monoesters? We considered two general mechanisms for the greater reactivity of Sp**U**pS as compared to p**U**p^{-4} using the standard TMN buffer conditions at pH 8.0: unfavorable electrostatic effects for the tetraanion and additional binding interactions of the hydroxypropyl substituent groups that serve to lower the activation barrier for Sp**U**pS. To evaluate the relative importance of these two possible mechanisms, we investigated the pH and salt dependence of the reactions.

The pH dependence of k_{cat}/K_m for p**U**, **U**p, **U**p, and Sp**U**pS was investigated in the pH range of 6.0−9.0 (Figure 5A). In this range, the rates for p**U** and **U**p show no significant changes (<1.6-fold), while Sp**U**pS shows a modest 4.5-fold decline when the pH is lowered from 8 to 6. These results show that there are no essential groups on free UDG that titrate in this range. In contrast, p**U**p shows a 30-fold decline in rate as the pH is increased from which a pK_a of 7.5 ± 0.2 was determined (Figure 5A). This pK_a is similar to the pK_a of 7.1 ± 0.1 for deprotonation of the 3′- and 5′-phosphate monoanions as determined directly using ^{31}P NMR (Figure 5B). The good agreement between the NMR and kinetic pK_a values strongly suggests that the removal of a proton from the 3′- and 5′-phosphates leads to a less reactive ionic form of the substrate p**U**p. [If the ratio $(k_{cat}/K_m^{pUp})/(k_{cat}/K_m^{pU})$ is plotted vs pH, to compensate for small pH-dependent changes in enzyme activity, a pK_a of 7.1 ± 0.15 is obtained, which is identical to the NMR values.] We conclude that substrates containing a *single* phosphate monanion or dianion in the +1 or −1 position react equally with UDG (i.e., p**U** or **U**p), but that a substrate such as p**U**p with *two dianionic* phosphates is catalytically impaired at pH values above the phosphate pK_a.

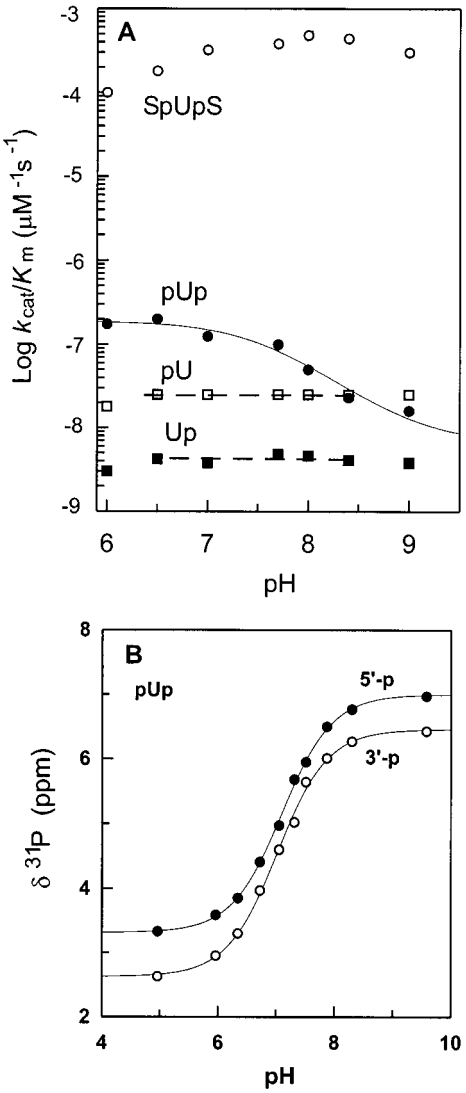

FIGURE 5: (A) pH dependence of k_{cat}/K_m for the indicated substrates. The solid line is a fit to eq 3 (pK_a = 7.5 ± 0.2), and the dashed lines are drawn to illustrate the pH independence of the reactions of p**U** and **U**p. (B) Determination of the pK_a values for the 3′- and 5′-phosphate groups of p**U**p using ^{31}P NMR. The lines are fits to eq 4 which gives pK_a values of 7.1 ± 0.1 for both phosphates.

The k_{cat}/K_m for the substrate p**U**p also shows a unique sensitivity to $MgCl_2$ and NaCl concentrations (Figure 6). With increasing concentrations of $MgCl_2$ in the range of 0−40 mM, the rate for p**U**p *decreases* by 20-fold in a hyperbolic fashion, with an apparent K_D^{Mg} of 3.2 ± 0.3 mM (Figure 6A). This is a much steeper dependence on divalent cation concentration than is seen for either p**U** or **U**p, which have estimated K_D^{Mg} values of >30 and 18 mM, respectively. Moreover, the substrate Sp**U**pS shows almost no change in k_{cat}/K_m over the same $MgCl_2$ concentration range. These results indicate that Mg^{2+} binds to p**U**p differently than either of the other substrates. This mode of binding may involve a bridging interaction of Mg^{2+} through coordination of two or more oxygen atoms of the +1 and −1 phosphate groups.

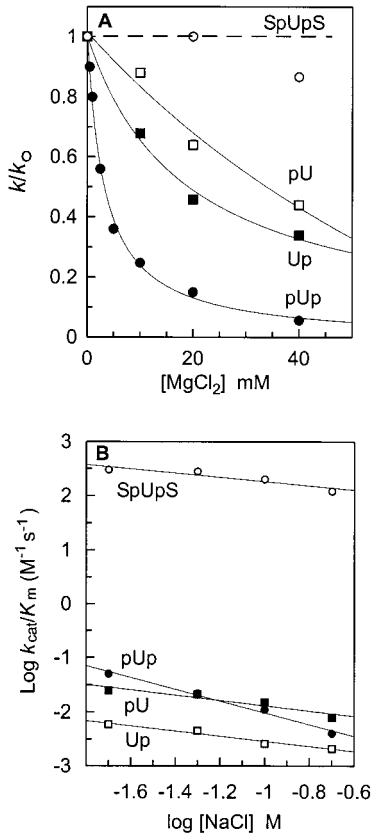

FIGURE 6: Dependence of k_{cat}/K_m on $MgCl_2$ and NaCl concentration. (A) Plot of the relative k_{cat}/K_m values as a function of $MgCl_2$ concentration. The solid lines are the fits to eq 5. The dashed line is drawn to illustrate the small $MgCl_2$ concentration dependence of k_{cat}/K_m for Sp**U**pS. The K_D^{Mg} values obtained from these fits were as follows: 3.2 ± 0.35 mM for p**U**p, >30 mM for p**U**, and 18 ± 7 mM for **U**p. (B) Log−log plot of the k_{cat}/K_m values for the indicated substrates as a function of log[NaCl]. The solid lines are the linear regression fits to eq 6 with the following fitted values: Sp**U**pS, $S = -0.4 \pm 0.1$ and $A = 1.8 \pm 0.14$; p**U**p, $S = -1.1 \pm 0.1$ and $A = -3 \pm 0.2$; **U**p, $S = -0.48 \pm 0.1$ and $A = -3 \pm 0.12$; and p**U**, $S = -0.49 \pm 0.2$ and $A = -2.4 \pm 0.2$.

Such an interaction in the free substrate could stabilize a conformation of p**U**p that is less reactive than the metal free form. As noted above, the greater extent of inhibition of the k_{cat}/K_m for p**U**p^{-4} at 2.5 mM $MgCl_2$ used in the standard TMN buffer contributes to the apparent negative cooperativity of binding the two phosphate groups.

As shown in Figure 6B, the power dependence of log k_{cat}/K_m on log[NaCl] was also steeper for p**U**p, with a slope S of -1 ± 0.1 (eq 6), suggesting that the observed inhibition involves competition by a single sodium ion for a phosphate binding site (*20*). For the substrates p**U**, **U**p, and Sp**U**pS, the power dependence of log k_{cat}/K_m on log[NaCl] was shallower ($S \sim -0.5$), indicating a weaker competitive effect than for p**U**p. These studies of the salt dependence of k_{cat}/K_m indicate that divalent cation binding or ionic screening of the phosphate groups of p**U**p cannot substitute for the activation provided by specific protonation.

Since simply protonating the phosphate groups of p**U**p^{-4} increases its reactivity by ~30-fold (2 kcal/mol), as estimated from the limiting pH-dependent k_{cat}/K_m values (Figure 5A), it seems likely that unfavorable charge effects do play a role in its decreased reactivity. We envision at least three mechanisms that could produce this result. First, the average solution conformation of p**U**p^{-4} could be less reactive than p**U**p^{-2}. We consider this an unlikely mechanism, however, because the average conformations of the 3′- and 5′-monophosphates and 3′,5′-diphosphates of thymidine are similar and essentially independent of pH as determined from NMR measurements (*23*). Alternatively, hydrogen bonds from active site donors such as Ser88 and Ser189 could be weakened due to the altered charge distribution and P−O bond lengths in p**U**p^{-4} as compared to p**U**p^{-2}, giving rise to a less favorable binding mode for p**U**p^{-4} (see Figure 1). Finally, electrostatic strain between the highly charged +1 and −1 phosphates of p**U**p^{-4} could contribute to its ~2 kcal/mol greater barrier than p**U**p^{-2} if the phosphate binding sites have an effective dielectric constant lower than that of water. The relatively modest 2 kcal/mol benefit of adding two protons to p**U**p^{-4} establishes that the 6.9 kcal/mol benefit (110000-fold) of adding the two S substituents to p**U**p^{-4} is largely due to additional binding interactions with the flexible hydroxypropyl substituents.

Coupling Energy Analysis of the Combined +1 and −1 Interactions in the 3mer Scaffold. The combined energetic effect ($\Delta\Delta G_{both}$) of adding two substituent groups such as protons, S, or D at the +1 and −1 positions may be the simple sum of the energetic contributions of the individual groups ($\Delta\Delta G_1 + \Delta\Delta G_2$), or may differ from additivity by the coupling energy between the groups (ΔG_c, eq 3) (*24*).

$$\Delta\Delta G_{both} = \Delta\Delta G_1 + \Delta\Delta G_2 + \Delta G_c \qquad (7)$$

Thus, the coupling energy may be calculated by subtracting the two individual effects on the catalytic efficiency from the combined effect [$\Delta G_c = \Delta\Delta G_{both} - \Delta\Delta G_1 - \Delta\Delta G_2$, where $\Delta\Delta G_x = -RT \ln CE^x/CE^{hUh}$ and $x = 1$, 2 or both]. In the present case, the combined addition of a +1 and −1 phosphate monoanion results in a substrate, p**U**p^{2-}, that is −1.64 kcal/mol *more* efficient than expected from the additive effects of the individual +1 and −1 phosphate monoanions, indicating cooperative binding of the two phosphate monoanion groups. In contrast, addition of a +1 and −1 phosphate dianion to form p**U**p^{4-} results in a substrate that is +0.44 kcal/mol *less* efficient than expected from additive effects, indicating anticooperative binding of the dianions. [We should point out that the above energetic comparisons are made from the kinetic measurements in the *absence of $MgCl_2$* (10 mM buffer and 20 mM NaCl), which negates complications from the differing inhibitory effects of this divalent salt.] Overall, protonation of the +1 and −1 phosphate groups decreases the coupling energy term by −2.1 kcal/mol (−1.64 to 0.44). Since these substrates differ only by protonation of two phosphate oxygens, it is reasonable to interpret this more negative coupling energy as the net electrostatic effect of removing two negative charges from p**U**p^{4-}.

Combined addition of a +1 and −1 phosphodiester to h**U**h yields substrates that are −0.7 kcal/mol (Dp**U**pD) and −1.2 kcal/mol (Sp**U**pS) *more* efficient than expected from the additive effects of the +1 and −1 S and D substituents, also indicating cooperative binding. Although addition of the D and S groups results in much larger 8000- and 170000-fold rate enhancements compared to the 2−15-fold effects of adding +1 and −1 phosphate monoanions, the coupling energies for both free energy cycles are essentially the same

(−0.7 to −1.6 kcal/mol). These similar values suggest that the favorable coupling energy for binding two phosphate monoanions or diesters at the +1 and −1 positions arises from the similar chemical character of these phosphoesters, and not from interactions of UDG with the different substituent groups (protons, S, or D).

Role of the +1 and −1 Nucleotides in the Context of a 4mer Scaffold. Systematic removal of the base, furanose, and phosphoester moieties at the +1 position of Ap**U**pApA indicates that (i) the +1 base is involved in ground-state binding, (ii) the + 1 furanose group provides most of the binding interactions required to lower the activation barrier described by k_{cat}, and (iii) the +1 phosphate stabilizes the ground state, but does not serve to lower the activation barrier (Table 1). Thus, these results indicate that the catalytically important binding interactions with the +1 nucleotide handle do not involve the base moiety, and are nearly maximal when the +1 substituent possesses a furanose sugar. The net contribution of the +1 nucleotide (Ap) to catalysis is about 3300-fold (−4.8 kcal/mol) as judged by comparison of the CE values for Ap**U**pApA and h**U**pApA.

Pivotal Role of the −2 Phosphoester Handle. Dramatic evidence for the importance of the −2 phosphoester or nucleotide is the enormous 20000- and 270000-fold increases in CE upon addition of a −2 phosphate and pA nucleotide to Ap**U**pA to form Ap**U**pAp and Ap**U**pApA, respectively (Table 1). These effects correspond to apparent interaction energies of −5.9 and −7.5 kcal/mol for the −2p and −2 pA groups, respectively (Table 1).[1] In contrast with the effects of proton, D, and S substituents at the +1 and −1 positions, there is no large difference in CE between a phosphate dianion, pS, or pD substituent at the −2 position (compare the CE values for Ap**U**pAp, Ap**U**pApS, and Ap**U**pApD in Table 1). However, addition of the complete −2 nucleotide (pA) produces a 14-fold larger rate enhancement than the phosphate dianion alone. The crystal structures of *h*UDG and *e*UDG bound to dU-containing DNA (*4*, *5*, *7*), and the two-dimensional representation shown in Figure 1 suggests a structural basis for the large catalytic effect of the −2 phosphoester. The nonbridging oxygens of this group are hydrogen bonded to the backbone amide groups of the catalytic electrophile His187, and conserved residue Ser166. We envision these −2 interactions are essential for driving the active site into the productive closed conformation (*7*), allowing formation of the strong hydrogen bond between uracil O2 and His187, and optimizing the interactions at the +1 and −1 positions as described further below.

Comparison of the net catalytic benefit imparted by the −2 nucleotide handle when this group is appended onto the substrate Dp**U**pD or Sp**U**pS provides additional insights into the requirements for effective transmission of the binding energy provided by this handle. Without the −2 pA handle, Dp**U**pD is found to be a 20-fold poorer substrate than Sp**U**pS ($\Delta\Delta G^{\ddagger} = \Delta G^{\ddagger}_{DUD} - \Delta G^{\ddagger}_{SUS} = 1.8$ kcal/mol). Thus, the simpler and more flexible S substituents are more effective in lowering the activation barrier than the D substituents in this context. However, the situation is reversed when the −2 pA group is added to Dp**U**pD and Sp**U**pS, where the rate for Dp**U**pDpA is about 9-fold greater than that for Sp**U**pSpA. The above observations indicate that Dp**U**pD is incapable of attaining its full binding interactions with UDG in the absence of the −2 pA substituent. Thus, this handle may serve to drive the rigid D substituent groups into their optimal binding arrangement, resulting in additional binding interactions with the sugar rings that lead to the observed 1300-fold rate enhancement over Dp**U**pD (−4.3 kcal/mol). The catalytic effect of the −2 pA is even larger when appended to Ap**U**pA (−7.5 kcal/mol), reflecting the additional binding interactions obtained from the complete nucleotides in the +1 and −1 positions. In contrast, addition of the −2 handle to Sp**U**pS only provides an 8-fold rate enhancement (1.2 kcal/mol). A possible explanation for these differential effects is that full utilization and transmission of the binding energy of the −2 handle requires rigid furanose ring systems or nucleotides in the +1 and −1 positions.

Table 2: Base Sequence Effects on the Kinetic Parameters for Uracil Cleavage[a]

substrate	k_{cat} (s^{-1})	K_m (μM)	k_{cat}/K_m (μM^{-1} s^{-1})
ApUpApA	15.81 ± 0.33	1.04 ± 0.09	15.20 ± 1.36
ApUpPpA	13.51 ± 0.87	4.66 ± 0.90	2.90 ± 0.59
CpUpCpC	27.08 ± 0.87	1.36 ± 0.17	19.94 ± 2.62
GpUpGpG	24.53 ± 0.55	3.44 ± 0.26	7.14 ± 0.56
TpUpTpT	20.24 ± 1.38	2.71 ± 0.65	7.46 ± 1.86

[a] Kinetic parameters were determined at 25 °C in TMN buffer at pH 8.0.

Are Bases Important in Binding or Catalysis? The data in Table 1 clearly show that removing a single base from the +1, −1, or −2 position by substitution of D has little effect on k_{cat}. (The true effects may be somewhat larger since k_{cat} is limited by product release and not chemistry for Ap**U**pApA.) In contrast, removal of the base does have a significant effect on binding as judged by the 3-, 172-, and 64-fold larger K_m values when adenine is deleted from the +1, −1, and −2 positions, respectively. The +1 and −1 effects are energetically additive, as the product of the individual K_m effects (530-fold) approximates that of the combined effect for Dp**U**pDpA (937-fold). Interestingly, these data provide no evidence for tight binding of UDG to the abasic sites in these constructs, as has been reported for the human enzyme with duplex abasic DNA (*4*, *5*). Such an effect should appear as nonproductive binding, leading to lower k_{cat} values, which is clearly not observed. The significantly weaker binding of UDG to these single-stranded DNAs with abasic sites in the +1, −1, or −2 position suggests that uracil sites adjacent to already existing abasic sites may not be efficiently repaired by the enzyme. These results may reflect on the reaction of UDG on single-stranded DNA regions that occur during replication or transcription.

We also investigated base specific effects at the +1, −1, and −2 positions by substituting C, G, T, and the unnatural base 2-aminopurine (P). A similar trend was observed as for the abasic constructs, where k_{cat} was essentially unchanged for the series, but K_m values varied as much as 4.5-fold in the following order: A < C < T < G < P (Table 2). We have noted a similar trend of base specific effects in a more limited steady-state kinetic study using 19mer duplex DNA substrates. In this work, the K_m values for sequences containing G·C and C·G base pairs flanking the deoxyuridine were lower by about 10-fold compared to those of A·T base pairs, but similar k_{cat} values were observed (not shown). A detailed accounting for the weaker binding of duplex DNA containing G·C and C·G base pairs has not been completed, but recent stopped-flow kinetic studies indicate a greater

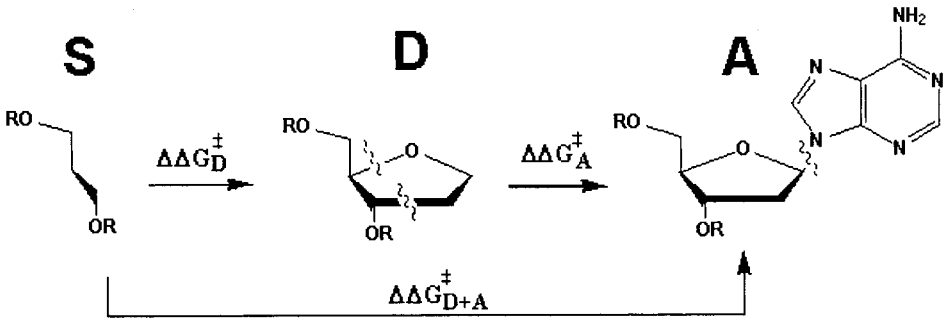

Position (x = D or A)	ΔΔG‡D (kcal/mol)	ΔΔG‡A (kcal/mol)	ΔΔG‡D+A (kcal/mol)	Important Interaction
+1 SpUpApA → XpUpApA	-0.7	-0.7	-1.4	Furanose and Base
-1 ApUpSpA → ApUpXpA	-0.1	-3.4	-3.5	Base
-2 ApUpApS → ApUpApX	0	-1.9	-1.9	Base

FIGURE 7: Difference free energies for the addition of furanose (D) and adenine (A) groups at the +1 position of Sp**U**pApA, −1 position of Ap**U**pSpA, and −2 position of Ap**U**pApS. These difference free energies were calculated using the equation $\Delta\Delta G^{\ddagger}_{D} = -RT \ln(k_{cat}/K_m)^X/(k_{cat}/K_m)^S$, where $(k_{cat}/K_m)^X$ is the parameter for the substrate with D or A in the +1, −1, or −2 position and $(k_{cat}/K_m)^S$ is the value for the corresponding substrate with S in the same position. The errors in the difference free energies are less than ±0.3 kcal/mol. The important interactions based on this analysis are indicated.[1] The incremental effect of the base and sugar in the +1 position is small (−1.4 kcal/mol) compared to the importance of the entire Ap substituent (−4.9 kcal/mol; see Table 1).

kinetic barrier for association of the enzyme with these DNA constructs (J. T. Stivers, unpublished observations). Although these base specific effects appear to be similar for single-stranded and duplex DNA, it seems likely that the molecular details that determine the reactivity of these DNAs will differ because of the large structural differences in these substrates.

The observation of small base specific effects on k_{cat} is consistent with the expectation that evolution would select for catalytic machinery that is insensitive to such effects, because, as guardians of the genome, repair enzymes should act with equal proficiency on a damaged site regardless of its sequence context. The modest base specific differences in K_m values for both single-stranded and duplex DNA constructs suggest that the DNA substrate may be present in sufficient concentration in vivo to saturate the enzyme, thus removing further selective pressure to equalize binding affinities for all sequences.

The free energy changes (derived from the k_{cat}/K_m measurements) of systematically adding a furanose sugar ring (D), base (A), or both a sugar and base (D + A) in the +1, −1, and −2 positions are shown in Figure 7. These difference free energies, which are relative to substrates with an S substituent in the +1 and −1 positions, quantify the relative importance of furanose and base interactions at these three positions. This analysis indicates that at the −1 and −2 positions the base interactions are important for catalysis, but at the +1 position, sugar and base interactions contribute in an additive fashion.

We have summarized the important substrate binding energy contributions to catalysis in Figure 8. Although none of these interactions, singly or in pairs, contribute more than −7 to −8 kcal/mol toward the catalytic efficiency, the net energetic contribution of adding +1, −1, and −2 nucleotides to h**U**h is worth an impressive −13 kcal/mol. These experimental findings provide energetic boundaries to guide further evaluation of the relative contributions of ground-state destabilization and transition-state effects in the catalytic mechanism of this fascinating enzyme.

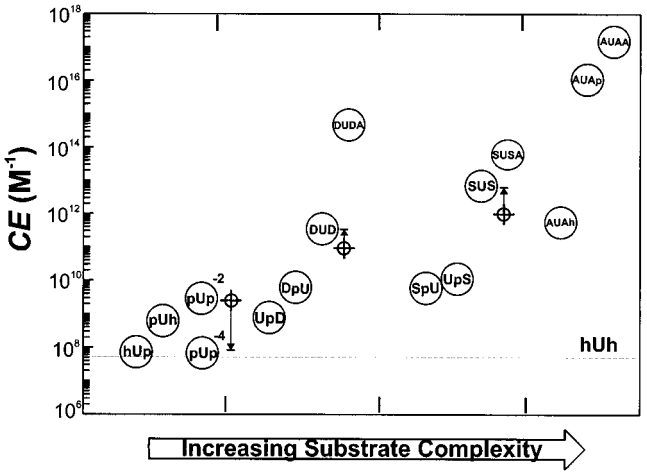

FIGURE 8: Reconstructing the substrate of UDG. The catalytic efficiencies (CE) of selected substrates from Table 1 are shown. The horizontal dashed line is drawn at the CE value for the minimal substrate h**U**h. The arrows show the deviation from additivity for the addition of two phosphate dianions, or S or D groups at the +1 and −1 positions, compared to the additive free energy effects for addition of the single substituents at each position (see the text). CE values for the dianion and tetraanion forms of p**U**p are given. These data were extrapolated from the low- and high-pH asymptotes of the pH dependence of k_{cat}/K_m according to eq 3 (see Figure 5A). The net energetic contribution of adding +1, −1, and −2 nucleotides to h**U**h is worth an impressive four billion-fold to catalysis (−13.2 kcal/mol).

ACKNOWLEDGMENT

We thank Dr. Fenghong Song for the synthesis and characterization of the DNA substrates used in these studies and Drs. Alex Drohat and Burkhard Luy for assistance with the ^{31}P NMR experiments.

REFERENCES

1. Snider, M., Gaunitz, S., Ridgway, C., and Wolfenden, R. (2000) *Biochemistry 39*, 81.
2. Bruice, T. C., and Benkovic, S. J. (2000) *Biochemistry 39*, 6267−6274.
3. Jencks, W. P. (1975) *Adv. Enzymol. Relat. Areas Mol. Biol. 43*, 219−410.
4. Parikh, S. S., Mol, C. D., Slupphaug, G., Bharati, S., Krokan, H. E., and Tainer, J. A. (1998) *EMBO J. 17*, 5214−5226.
5. Parikh, S. S., Walcher, G., Jones, G. D., Slupphaug, G., Krokan, H. E., Blackburn, G. M., and Tainer, J. A. (2000) *Proc. Natl. Acad. Sci. U.S.A. 97*, 5083−5088.
6. Betts, L., Xiang, S. B., Short, S. A., Wolfenden, R., and Carter, C. W. (1994) *J. Mol. Biol. 235*, 635−656.
7. Werner, R. M., Jiang, Y. L., Gordley, R. G., Jagadeesh, G. J., Ladner, J. E., Xiao, G., Tordova, M., Gilliland, G. L., and Stivers, J. T. (2000) *Biochemistry 39*, 12585−12594.
8. Stivers, J. T., Pankiewicz, K. W., and Watanabe, K. A. (1999) *Biochemistry 38*, 952−963.
9. Drohat, A. C., and Stivers, J. T. (2000) *J. Am. Chem. Soc. 122*, 1840−1841.
10. Drohat, A. C., and Stivers, J. T. (2000) *Biochemistry 39*, 11865−11875.
11. Dong, J., Drohat, A. C., Stivers, J. T., Pankiewicz, K. W., and Carey, P. R. (2000) *Biochemistry 39*, 13241−13250.
12. Werner, R. M., and Stivers, J. T. (2000) *Biochemistry 39*, 14054−14064.
13. Fasman, G. D. (1975) *Handbook of Biochemistry and Molecular Biology: Nucleic Acids*, 3rd ed., Vol. 1, CRC Press, Boca Raton, FL.
14. Drohat, A. C., Jagadeesh, J., Ferguson, E., and Stivers, J. T. (1999) *Biochemistry 38*, 11866−11875.
15. Xiao, G., Tordova, M., Jagadeesh, J., Drohat, A. C., Stivers, J. T., and Gilliland, G. L. (1999) *Proteins 35*, 13−24.
16. Leatherbarrow, R. J. (1998) *Grafit 4*, Erithacus Software Ltd., Staines, U.K.
17. Stivers, J. T., Abeygunawardana, C., Mildvan, A. S., Hajipour, G., and Whitman, C. P. (1996) *Biochemistry 35*, 814−823.
18. Record, M. T., Ha, J.-H., and Fisher, M. A. (1991) *Methods Enzymol. 208*, 291−343.
19. Shapiro, R., and Kang, S. (1969) *Biochemistry 8*, 1806−1810.
20. Shapiro, R., and Danzig, M. (1972) *Biochemistry 11*, 23−29.
21. Fersht, A. (1985) *Enzyme Structure and Mechanism*, W. H. Freeman and Co., New York.
22. Varshney, U., and van de Sande, J. H. (1991) *Biochemistry 30*, 4055−4061.
23. Niemczura, W. P., and Hruska, F. E. (1980) *Can. J. Chem. 58*, 472−478.
24. Mildvan, A. S., Weber, D. J., and Kuliopulos, A. (1992) *Arch. Biochem. Biophys. 294*, 327−340.

BI010622C